ZM6镁合金铸件 TIG焊补焊工艺

王 欣[1], 杨 闯[2], 冯吉才[1]
(1. 哈尔滨工业大学 材料科学与工程学院, 哈尔滨 150001;
2. 黑龙江工程学院 材料与化学工程系, 哈尔滨 150050)

王 欣

摘 要: 根据拉伸性能测试结果及 X射线探伤检测确定了 ZM6镁合金铸件 TIG焊补焊工艺参数. 并通过光学显微镜对焊接接头进行了微观组织观察和微区成分分析试验. 结果表明, 热影响区晶粒大小与母材基本相同. 在热影响区晶内完全由 Mg元素组成, 晶内原有的合金元素迁移到晶界. 焊缝组织由比母材晶粒尺寸小的细小等轴晶组成, 焊缝区的晶内组织基本由 Mg元素组成, 其晶界合金元素含量要比母材与热影响区少. 通过对 ZM6镁合金铸件补焊中的裂纹位置以及成分分析, 得出 ZM6镁合金铸件补焊裂纹为结晶裂纹.

关键词: ZM6镁合金铸件; TIG焊补焊; 工艺方法
中图分类号: TG115.28 文献标识码: A 文章编号: 0253-360X(2010)09-0033-04

0 序 言

镁合金作为目前世界上最轻质的工程结构金属材料之一, 具有密度低、比强度和比刚度高等优点, 被誉为“21世纪绿色结构材料”, 具有广泛应用于航空航天、国防军工、交通运输等领域的潜力[1]. 中国是世界上镁资源最为丰富的国家之一, 总储量占世界 22.5%, 居世界第一. 高质、高效焊接技术较其它成形技术发展缓慢的现状已经成为严重制约中国镁合金广泛应用的瓶颈之一, 这主要是由于镁合金焊接过程中易产生热裂纹、气孔、氧化物夹渣以及脆性氮化物降低接头性能等问题. 交流 TIG焊接是目前实际应用于镁合金连接的主要电弧焊方法[2-6]. 镁合金在铸造成形过程中, 不可避免的产生各种缺陷, 如夹杂、冷隔、气孔和裂纹等, 对缺陷铸件进行挽救修复具有重大的经济意义, 这些缺陷主要以补焊手段来弥补.

根据 ZM6镁合金铸件组织, 制定了 TIG填丝补焊工艺, 通过补焊接头性能测试及着色检查, 优化了 ZM6镁合金铸件 TIG填丝补焊工艺参数, 并进一步分析 ZM6镁合金铸件补焊接头组织特征, 通过观察接头组织特征得出镁合金铸件补焊接头裂纹形成的原因, 以此减少 ZM6镁合金铸件补焊中裂纹的产生, 实现了 ZM6镁合金铸件的修复.

1 试验方案

1.1 试验材料

试验母材为 ZM6镁合金铸件, 化学成分如表 1所示, 铸件微观组织如图 1所示, 其抗拉强度和断后伸长率分别为 160 MPa和 3.3%. 由表 1可以看出, 镁合金铸件的主要合金元素为 RE, 其中, RE为含有 Nd元素不小于 85% (质量分数)的钕混合稀土.

表 1 ZM6铸件镁合金的化学成分(质量分数, %)
Table 1 Chemical composition of ZM6 magnesium alloy

RE	Zr	Zn	Cu	Ni	杂质	Mg
2.0~2.8	0.4~1.0	0.2~0.7	0.10	0.01	0.30	余量

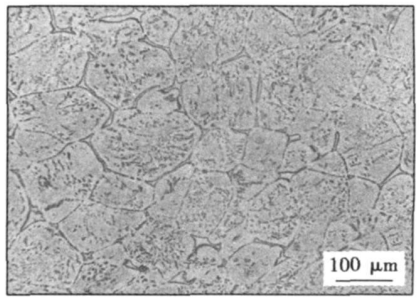

图 1 ZM6镁合金铸件微观组织
Fig. 1 Microstructure of castings in ZM6 magnesium alloy

收稿日期: 2010-05-18
基金项目: 国家 863高技术研究发展计划资助项目(2002AA331160)

补焊过程中使用的焊丝材料与母材同质.

1.2 试验方案

对 ZM6镁合金铸件缺陷进行补焊,补焊的缺陷主要是未充满和气孔,保护气体选用工业用普通氩气,补焊工作场地温度不应低于 15 ℃,且不应有空气流通.试验研究采用 5种焊接工艺方案,氩气流量 10 L/min,喷嘴直径为 12 mm,钨极直径 3 mm,制定的补焊工艺参数如表 2所示,在其中选取最优的工艺组合.为防止补焊裂纹和其它缺陷的产生,焊前对焊丝表面、焊接坡口及其附近部位进行严格的化学、机械清理.

表 2 ZM6镁合金补焊工艺参数

Table 2 Welding parameters of ZM6 magnesium alloy

方案	焊接电流 I/A	电弧长度 L/mm	焊丝直径 D/mm	预热温度 T/℃
1	直流 250	3~4	3	无预热
2	交流 200	3~4	5 5	120
3	交流 200	3~4	4	230
4	交流 180	3~4	4	150
5	交流 180	2~3	5 5	230

方案 1和方案 2采用单层补焊,从方案 3开始,将单层补焊改为打底加盖面的双层焊;方案 4为相对于焊接面开上大下小的 V形坡口,并在收弧时电流缓降且多填丝;而方案 5采用手工打磨开设收弧槽,实现缝外收弧,以降低形成裂纹的倾向.焊后利用 INSTRON-5569电子万能试验机(抗拉强度取 3个试样的平均值)测试焊接接头的力学性能,焊缝位于拉伸试样中心,拉伸试件几何尺寸如图 2所示.采用光学显微镜、Hitachi-4700型扫描电子显微镜附件能谱仪分析焊缝微观组织.

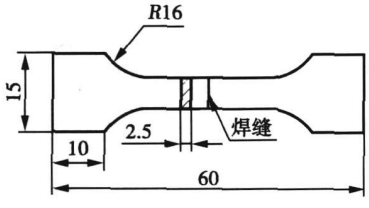

图 2 拉伸试样的几何尺寸(mm)

Fig. 2 Geometry size of tensile testing specimen

2 试验结果及讨论

2.1 补焊方案的确定

分别按照表 2所示的 5种工艺方案对 ZM6镁合金铸件缺陷进行补焊试验,并对焊缝进行力学性能测试以及着色检查.5种补焊方案补焊接头的拉伸性能如图 3所示.可以看出,在 5种方案中,按照方案 5进行补焊接头的性能最好,抗拉强度和断后伸长率分别为 150 MPa和 3.6%,抗拉强度达到母材的 94%,而断后伸长率比母材略高.方案 2~4的补焊接头的性能比较接近.方案 1补焊接头性能最差,抗拉强度和断后伸长率分别只有 63 MPa和 0.7%.补焊接头的性能测试证实了方案 5为补焊 ZM6镁合金铸件缺陷的最佳选择.分别对 5种补焊接头进行着色检验显示,按照方案 1进行的试验,补焊接头主要是熔合区裂纹和焊缝表面裂纹,以及熔合区和焊缝中的未熔合缺陷,且缺陷尺寸较大.而按照方案 2~4进行的试验,缺陷类型为未熔合缺陷,并且随着焊接工艺的调整,缺陷尺寸逐渐缩小.进一步按照方案 5进行试验,补焊完成后,经着色检验,表明焊缝外观成形良好,方案 5补焊焊缝外观如图 4所示.这主要是方案 5的试件预热温度高于方案 4,且焊丝直径大于方案 4,电弧长度较小(2~3 mm),相同的保护气体流量下,具有更好的保护效果;另外,由于焊丝直径较粗,在相同送丝速度下,熔化焊丝的能量就越多,因而母材吸收的能量相应减少,熔池过热度降低,从而降低了热裂纹产生的倾向性.得出方案 5的焊缝质量良好,未产生裂纹.

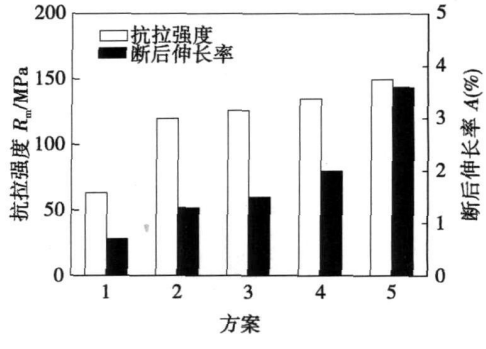

图 3 补焊接头的拉伸性能

Fig. 3 Tensile properties of welding joints

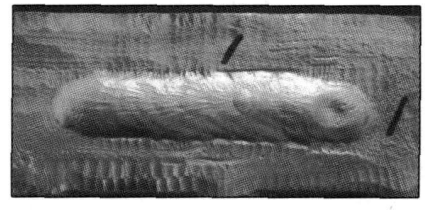

图 4 焊缝外观

Fig. 4 Weld appearance

通过以上试验研究确定 ZM6镁合金铸件补焊

工艺为普通交流电源、氩气保护、焊前预热及双层焊接，具体工艺参数如表 2中方案 5所示.

2.2　补焊接头的组织特征分析

图 5为 ZM6镁合金铸件按照方案 5进行补焊接头微观组织. 表 3为通过能谱分析所得的焊接接头和母材化学成分分布. 图 5(a)所示为镁合金铸件补焊接头焊缝与热影响区界面附近的微观组织. 可以看出，热影响区晶粒仍然为等轴晶. 与母材(图 1)相比较，热影响区晶粒大小与母材基本相同，即经过补焊之后，热影响区晶粒并没有发生一般焊接接头所出现的晶粒粗化倾向. 但是，由表 3可以看出，热影响区与母材不同的是，其晶内完全由 Mg元素组成，也就是说，在热影响区，晶内原有的合金元素向晶界偏析，晶内由于快速的选择结晶而不含合金元素. 此外，热影响区晶界的化学成分与母材晶界基本相同，但由于热影响区晶内合金元素向晶界的偏析而使晶界化合物含量稍有增加.

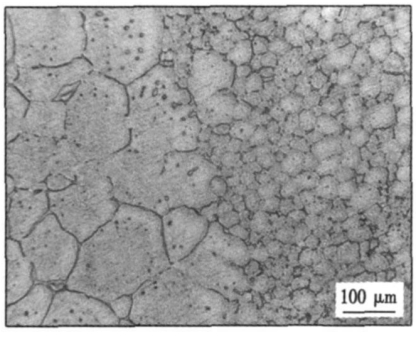

(a) 焊缝和热影响区界面

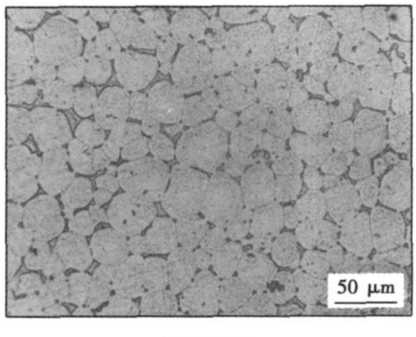

(b) 焊缝区

图 5　焊缝和热影响区界面的微观组织

Fig. 5　Microstructure between weld nugget and heat affected zone

图 5(b)所示为镁合金铸件补焊接头焊缝中心部位的微观组织. 可以看出，焊缝组织均由等轴晶所组成，但焊缝晶粒比母材晶粒的尺寸小得多，为细小的等轴晶. 在焊缝区，由于焊接温度较高，焊缝区金属熔化后，在快速冷却过程中，由于镁合金导热系数大，散热快，使得焊缝区金属快速凝固结晶，从而导致了焊缝区的晶粒细化，因此在焊缝区得到细小的等轴晶.

表 3　焊缝和热影响区及母材的化学成分

Table 3　Chemical composition of weld nugget, heat affected zone and base materials

元素		质量分数(%)			原子分数(%)		
		Mg	Nd	Zn	Mg	Nd	Zn
焊缝	晶界	87.37	10.43	2.2	97.14	1.95	0.91
	晶内	100	—	—	100	—	—
热影响区	晶界	63.27	27.24	9.49	88.63	6.43	4.94
	晶内	100	—	—	100	—	—
母材	晶界	74.19	18.14	7.68	92.62	3.82	3.65
	晶内	96.91	1.52	—	99.31	0.26	—

2.3　补焊接头裂纹的形成

图 6给出方案 1补焊接头横截面上观察到的焊接裂纹. 由图 6(a)所示，裂纹出现的部位为焊缝的上表面. 由裂纹的放大图 6(b)可以清晰地看出裂纹已经形成，极大削弱了接头的力学性能和使用性能.

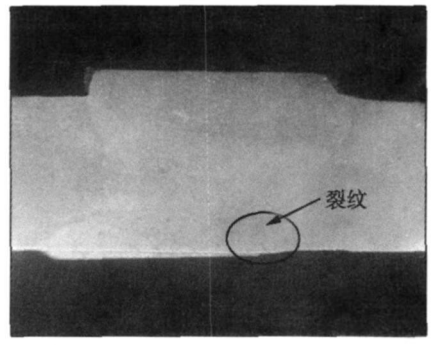

(a) 焊接裂纹位置

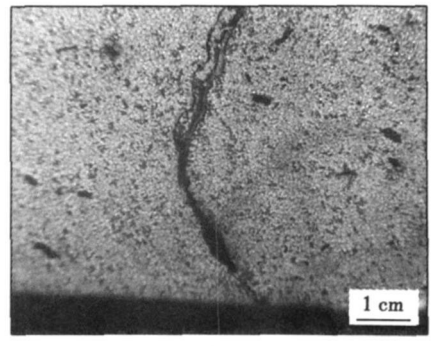

(b) 焊接裂纹形貌

图 6　焊接接头横截面上的焊接裂纹

Fig. 6　Welding crack in crosssection of welding joint

表 4所示为裂纹晶界处化学成分. 可以看出，合金元素含量远高于表 3中合金元素含量，由此可证明为结晶裂纹. 裂纹产生的原因为平衡状态下其结

晶过程中首先析出 α 固溶体，当温度达到共晶温度时，随着温度进一步降低，$Mg_{12}Nd$化合物开始析出，这个过程一直持续到室温. 因此，在这一范围的镁合金平衡结晶的室温组织理论上应当是 α 固溶体与 $Mg_{12}Nd$沉淀相. 而在实际的凝固条件下，由于镁合金的导热系数大，在焊后极冷条件下，会生成伪共晶组织. 到结晶后期，这种强度低且塑性差的低熔点共晶液态在晶界处最后凝固，已凝固的固态金属由于冷却收缩而对共晶成分的液态产生拉应力作用，当拉应力产生的塑性变形超过了液态薄膜所能承受的极限时，就会产生微裂纹. 当完全冷却后，应力进一步增大，微裂纹进一步扩展导致了裂纹的形成.

表 4 裂纹晶界处的化学成分

Table 4 Chemical composition of crystal in crack

元素	质量分数 (%)			原子分数 (%)		
	Mg	Nd	Zn	Mg	Nd	Zn
晶界	80.99	13.94	5.07	95.03	2.76	2.21

3 结 论

(1) 通过 5种工艺方案试验研究及拉伸性能测试数据验证，ZM6镁合金铸件补焊的具体工艺参数为普通交流电源 180 A，电弧长度 2～3 mm，氩气流量 10 L/min，焊丝直径 5.5 mm，焊前预热温度 230 ℃以及双层焊的焊接方法.

(2) 热影响区晶粒大小与母材基本相同，热影响区晶粒并没有发生一般焊接接头所出现的晶粒粗化倾向，焊缝组织为细小等轴晶.

(3) ZM6镁合金铸件补焊过程中的不平衡凝固，冷却速度较快引起明显的枝晶偏析，已凝固的固态金属冷却收缩对最后凝固共晶成分液体产生拉应力作用，导致裂纹的产生.

参考文献：

[1] 袁 泽，李德全，付 涛. 镁合金焊接技术的现状和发展趋势[J]. 现代焊接，2008，3：1－5.
Yuan Ze，Li Dequan，Fu Tao. The present situation and development trend of the welding technology of magnesium alloy[J]. Modern Welding Technology，2008，3：1－5.

[2] 柯黎明，邢 丽，徐卫平. AZ81A镁合金焊接接头的组织与性能[J]. 材料工程，2005，1：41－44.
Ke Liming，Xing Li，Xu Weiping. Microstructure and properties of welding joints for cast magnesium alloy AZ81A[J]. Journal of Materials Engineering，2005，1：41－44.

[3] 董长富，刘黎明，赵 旭. 变形镁合金填丝 TIG焊接工艺及组织性能分析[J]. 焊接学报，2005，26(2)：33－36.
Dong Changfu，Liu Liming，Zhao Xu. Welding technology and microstructure of tungsten inert-gas welded magnesium alloy[J]. Journal of Materials Engineering，2005，26(2)：33－36.

[4] 苗玉刚，刘黎明，赵 杰，等. 变形镁合金熔焊接头组织特征分析[J]. 焊接学报，2003，24(2)：63－66.
Miao Yugang，Liu Liming，Zhao Jie，et al. Microstructure feature analysis of fusion welded joint of wrought Mg alloy[J]. Transactions of the China Welding Institution，2003，24(2)：63－66.

[5] 刘政军，苏允海，李永奎，等. 镁合金焊接热裂纹机理的研究[J]. 热加工工艺，2006，35(7)：11－12.
Liu Zhengjun，Su Yunhai，Li Yongkui，et al. Study on mechanism of welding hot cracking for magnesium alloy[J]. Hot Working Technology，2006，35(7)：11－12.

[6] 王生希，宋 刚，刘黎明. 镁合金交流 TIG和脉冲 TIG组织性能分析[J]. 焊接学报，2006，27(9)：63－66.
Wang Shengxi，Song Gang，Liu Liming. Microstructure and property analysis of magnesium alloy welded with AC TIG welding and pulsed TIG welding[J]. Transactions of the China Welding Institution，2006，27(9)：63－66.

作者简介：王 欣，男，1974年出生，博士，现代焊接生产技术国家重点实验室博士后. 主要从事镁合金板材制备及焊接性方面的科研工作. 发表论文 4篇.

Email：xinwang@hit.edu.cn

Engineering, Guangdong University of Technology, Guangzhou 510006, China). p. 17—20

Abstract: The theory of stability of a liquid with free surface was applied to understand the instability phenomenon in bead formation. The experiment and analysis were carried out to discuss the effects on the bead formation for different current phases. The result showed that with the pulse current of the host and the accessory changed synchronously, the twin arc extinguished periodically. Then the heat which was transferred into the molten pool was decreased. This helped to avoid the molten pool to be too long and avoided the unstability of the liquid metal. When the pulse current of the host and the accessory changed alternately, the workpiece was heated by the arc throughout the welding process. As a result, the molten pool was very long which gave way to the unstability of bead formation and pinch effect of the liquid metal, so that it finally leaded to the humping phenomenon. When the pulse current phase of the host and the accessory changed indefinitely, the arc burned and extinguished in random. At the same time, the twin arc extinguished and the molten pool solidified in time. But when the twin arc extinguished, the molten pool could solidify in time and an uneven weld appearance was formed.

Key words: pulsed MAG welding; twin-wire co-pool; bead formation; current phase

An optimization algorithm for combination inverse kinematics problems of welding robot in complex trajectory

ZHOU Youhang, ZHANG Jianxun, DONG Yinsong (School of Mechanical Engineering, Xiangtan University, Xiangtan 411105, Hunan, China). p. 21—24

Abstract: To solve the combination problems of six DOF welding robot's inverse kinematics in complex trajectory planning, a variable step-size and revisable optimization algorithm was presented by building the nonlinear equations of robot kinematics models. Based on the conception of variable step and variable scale, the test strategy of forward-backward or maintain a step was adopted to approach the optimization objective for each joint under the given error, and the precision numerical solutions could be met after iterative searches. The computed conclusion showed that this method was effective and the program was easy to design. Moreover, the numerical solutions of the inverse kinematics could be optimized in nonlinear equations. At the same time, the stationary of six DOF welding robot joint movements in complex trajectory could be guaranted.

Key words: welding robot; inverse kinematics; variable step-size; complex trajectory planning

Microstructures and properties of CO_2 laser welded 600 MPa DP steel

WANG Wenquan1, MA Kai1, SUN Daqian1, KANG Chungyun2 (1. Key Laboratory of Automobile Materials, Jilin University, Changchun 130025, China; 2. Department of Electromechanical Engineering, Changchun Institute of Technology, Changchun 130015, China; 3. Department of Material Science and Engineering, Pusan National University, Pusan 609-735, Korea). p. 25—28

Abstract: CO_2 laser welding of cold rolled DP steel sheet with tensile strength of 600 MPa and thickness of 1.4 mm was carried out. The effects of welding speed on bead morphologies and cross-section shape were investigated. The microstructures of welded joint were observed. The hardness distribution, tensile strength and formability of the welded joint were tested. The study showed that for the same laser power, porosities occurred on weld bead at low welding speed and spatters occurred at high welding speed. In addition, welding speed also had influence on penetration and bead width. The weld metal was mainly composed of martensite due to high cooling rate of laser welding. The amount of martensite decreased rapidly approaching base metal from weld bead center. Therefore, the weld metal or heat affected zone had maximum hardness for the whole welded joint. The tensile strength of welded joint perpendicular to the weld line was equal to that of the base metal. But the tensile strength of welded joint parallel with the weld line was higher than that of the base metal. The plasticity and formability of the welded joint were impaired because of the formation of martensite in the weld metal.

Key words: laser welding; ultra-high strength steel; microstructure; fine texture; property

Control system designed for all position pipe welding device

LI Haichao, DU Lin, DONG Na, GAO Hongming (State Key Laboratory of Advanced Welding Production Technology, Harbin Institute of Technology, Harbin 150001, China). p. 29—32

Abstract: The pipe welding maintenance in nuclear environment requires the teleoperation method to be accomplished. According to the feature of the pipe maintenance in nuclear, the teleoperation control system was studied on the basis of the self-developed minor-caliber pipe welding device. The system was composed of the industrial computer in which the PC-6501D card was inserted. The signal of motor drivers was sent by the VC++ 6.0 programs to realize the motion of the whole system. To ensure the stability of the arc length during the all position welding and improve the quality of the welding, the close-loop feedback of the arc voltage was added in this system. Results show that the velocity and direction of the all position welding can be adjusted in this control system, moreover, the difference of the arc voltage was less than ± 0.2 V under the control of the arc length feedback. The actual welding results are satisfying.

Key words: remote welding; pipe welding; control system; arc length adjustment

Research on TIG repairing technology for ZM6 magnesium alloy casting

WANG Xin1, YANG Chuang1, FENG Jica1, 2 (1. School of Materials Science and Engineering, Harbin Institute of Technology, Harbin 150001, China; 2. School of Materials and Chemistry Technology, Heilongjiang Institute of Technology, Harbin 150001, China). p. 33—36

Abstract: The processing parameters of TIG repairing welding for ZM6 magnesium alloy casting were determined by testing tensile properties and X-ray. The same grain size between heat-affected zone and the base material was found by observing the microstructure of welded joints in the optical microscope and analysing micro-area composition. The element in the heat affected zone was basically occupied Mg, and the original crystal alloy elements within intragranular were migrated to the grain boundary. Weld was composed of small equiaxed crystal, the size of which was smaller than that in the base material. The grain in weld zone was also entirely occupied by Mg elements. The con-

tents of alloying elements in the grain boundary were less than those in the base material and heat-affected zone. The crystal cracks for welding in ZM6 magnesium alloy casting were found by observing the crack location and investigating the process of welding of ZM6 magnesium alloy casting.

Key words: ZM6 magnesium alloy casting; TIG repairing welding; process method

Effect of pulse current frequency on microstructure and mechanical properties of 2219 aluminum alloy weld joints

CONG Baoqiang, QI Bojin, LI Wei, YANG Mingxuan (School of Mechanical Engineering and Automation, Beihang University, Beijing 100191, China). p. 37—40

Abstract: The influence of pulse square-wave current frequency on the microstructure and mechanical properties of 2219 high strength aluminum alloy weld joints was investigated based on a novel ultrafast-convert hybrid pulse current variable polarity gas tungsten arc welding technique. The experimental results showed that comparing with no effect of pulse current, the coarse grains changed to fine equiaxed grains. A kind of finer equiaxed non-dentrites was observed distributing in the form of banding at the weld zone while the pulse current frequency was more than 20 kHz. Mechanical properties of weld joints were improved predominantly at the given pulse frequency of 60 kHz, tensile strength and percentage elongation of weld joints are increased by about 17.6% and 66%, respectively, compared to that of weld joints with no effect of pulse current. At the given pulse current amplitude and pulse duty cycle, with the pulse current frequency in certain range increased, the width of fusion zone obviously decreased and the ductility of welds was improved significantly. However, the variation in tensile strength of weld joints was relatively less sensitive with the increase of pulse current frequency.

Key words: high strength aluminum alloy; high frequency pulse current; pulse frequency; equiaxed non-dentrite; mechanical property

Formation characteristics of Ni/Ti intermetallics through annealing of layered Ni/Ti

ZHOU Yong-2, YANG Guan-Jun1, WU Xian2, LI Changjiu1 (1. State Key Laboratory for Mechanical Behavior of Materials, School of Materials Science and Engineering, Xi'an Jiaotong University, Xi'an 710049, China; 2. School of Materials Science and Engineering, Xi'an Shiyou University, Xi'an 710065, China). p. 41—44

Abstract: Ni/Ti diffusion couples were prepared by cold spraying with Ni and Ti powders and mechanically alloyed Ni/Ti alloy powders. The formation and growth characteristics of Ni/Ti intermetallics within Ni/Ti during solid state diffusion treatment were investigated by scanning electron microscopy (SEM) and X-ray diffraction (XRD). It was found that the thicknesses of Ni_3Ti, NiTi and Ti_2Ni intermetallic compounds layers increased with annealing temperature. The growth of TiNi layer followed the parabolic law with annealing time while the thicknesses of Ti_2Ni or Ni_3Ti layers were kept constant at certain annealing temperature. The results suggest that the formation and then rapid growth of TiNi intermetallic take place after Ni_3Ti and Ti_2Ni intermetallic compounds grow to certain thicknesses.

Key words: Ni/Ti diffusion couples; solid state diffusion; annealing treatment; intermetallic compound

Study of digital push-pull CO_2 welding system

LU Zhenyang, YAN Sibo, YANG Shuai, LIU Jia (College of Mechanical Engineering & Applied Electrons Technology, Beijing University of Technology, Beijing 100124, China). p. 45—48, 52

Abstract: The digital Push & Pull CO_2 welding system is proposed. This system utilize digital power source controlled by DSP and CPLD as platform with the AC servo push-pull feeder with the low moment of inertia, fast response, and steady feed speed. The constant feeding part combine with push-pull feeding part to form the whole feeder using buffer as a linker. Consider the characteristics of the push-pull short-circuit CO_2 welding technics, the feeder speed curve, welding voltage and current waveform control program was pre-designed. According to software program, the steady push-pull CO_2 welding technics was achieved with low spatter, low heat input and uniform droplet.

Key words: digital power source; push-pull feeder; CO_2 welding; low heat input

Study on structures and properties of part made by micro-plasma arc direct metal formation

XIANG Yonghua-2, XU Binshi1, LV Yaohui1 (1. Navy Logistic Technology and Equipment Institute of PLA, Beijing 100072, China; 2. National Key Laboratory for Remanufacturing, Academy of Armored Forces Engineering, Beijing 100072, China). p. 49—52

Abstract: The deposition experiments were done on the mild steel by micro-plasma arc powder overlaying rapid prototyping technique with Fe313 alloy powder. The microstructures and morphologies were observed by metallographic microscope and SEM, the microhardness was tested by vickers. It was showed that the middle layer displayed insular M-A component structure, and the interface between layers was evident. The microstructure of Fe-based deposited layer was affected by the subsequent overlaying with annealing process, and the crystalline grain refined. The hardness distribution curve of the cylindraceous part was as U shape, the middle layer was soften because the drawing effect of subsequent layers.

Key words: rapid prototyping; micro-plasma arc overlaying; Fe-based alloy; microstructure

Cracking formation mechanism of mild steel parts fabricated by surfacing rapid forming

LI Chao, LIANG Yuanyuan, SHEN Canduo, ZHU Sheng (National Defence Key Laboratory for Remanufacturing, Academy of Armored Forces Engineering, Beijing 100072, China). p. 53—56

Abstract: The micro-morphology of cracks for the parts fabricated by surfacing rapid forming was observed with SEM. The results showed that the cracks initiated from the first layer of the part, extended along the deposition direction, and finally terminated under the surface of the part. The segregation and inclusion in the formed part were studied by OM and EDS, moreover, the content of residual austenite was measured by XRD. The results indicated that the cracks were liquid hot cracks. In course of forming with multi-layers and multi-paths, the segregation comprised of Mn and Si oxidate, Mo carbide and Ni intermetallic compound were the internal cause for the cracks formation, while the tension stress was the external cause. By properly matching the contents of Mn, Ni and Si elements, purifying the weld metal with rear earth elements cerium, adopting the orthogonal deposi-